Journal of Power Sources 196 (2011) 6663–6669

Contents lists available at ScienceDirect

Journal of Power Sources

journal homepage: www.elsevier.com/locate/jpowsour

Observation of electrodeposited lithium by optical microscope in room temperature ionic liquid-based electrolyte

H. Sano[a,b], H. Sakaebe[a,b,*], H. Matsumoto[a,b]

[a] Research Institute for Ubiquitous Energy Devices, National Institute of Advanced Industrial Science and Technology (AIST), Midorigaoka 1-8-31, Ikeda, Osaka 563-8577, Japan
[b] Japan Science and Technology Agency, CREST, Midorigaoka 1-8-31, Ikeda, Osaka 563-8577, Japan

ARTICLE INFO

Article history:
Received 6 September 2010
Received in revised form
11 December 2010
Accepted 14 December 2010
Available online 23 December 2010

Keywords:
Lithium metal anode
Li rechargeable battery
Dendrite
Room temperature ionic liquids
Additive
In situ observation

ABSTRACT

Room temperature ionic liquids (RTILs) were applied to a lithium (Li) metal battery system, and the behavior of Li electrodeposition on nickel electrodes in RTILs was investigated using *in situ* optical microscopy with/without an organic additive, vinylene carbonate (VC), in the RTILs. Two RTILs, PP13[TFSA] (*N*-methyl-*N*-propylpiperidinium bis(trifluoromethanesulfonyl)amide) and EMI[FSA] (1-ethyl-3-methylimidazolium bis(fluorosulfonyl)amide), were chosen as the base electrolytes. Dendritic particles were obtained in the case of EMI[FSA] with and without VC, and PP13[TFSA] without VC, while non-dendritic fine particles were obtained in the case of PP13[TFSA] with VC.

1. Introduction

A sustainable society is one of the goals we, human beings, have to achieve. With regard to energy, the use of renewable energy is the most promising solution to realize such a society. A battery system promotes the strengths of renewable energy, as, for example, a battery can store the surplus energy from solar photovoltaic power generation in the daytime, and can discharge this power at night. Thus, a sustainable society requires battery systems. Of course, batteries are to be used not only in connection with power plants but also in mobile electric devices and in automobiles.

A long operating life and high energy density are key requirements for an innovative new battery. Lithium (Li) metal is attractive owing to its ability to realize a high cell voltage and high energy density, as is needed for the commercialization of the electric vehicle (EV). The biggest obstacle to the commercialization of a Li metal rechargeable battery is dendrite formation of Li metal during charging, which causes short circuiting and poor cycling properties [1].

Li dendrites are thought to grow because of nonuniform film on the Li metal surface formed when Li metal contacts the electrolyte solution [1]. The nonuniform film cracks and the Li deposits more near the cracks during charging. In another case, Li deposits more where the film is thinner. To alter the property of the surface film and improve the Li cycling efficiency, some research groups added organic or inorganic additives to the electrolyte [2–9].

At the same time, room temperature ionic liquids (RTILs), which are well-known for their thermal stability and non-flammability, have attracted much attention, because they improve the safety of the entire battery. Some groups including ours have already reported interesting results, which may hopefully solve the problem of Li dendrites [10–15]. Sakaebe et al. reported the marked efficiency of Li cycling in a specific RTIL, PP13[TFSA] (*N*-methyl-*N*-propylpiperidinium bis(trifluoromethanesulfonyl)amide), which has quaternary ammonium cations and high-level cathodic stability [15]. In this report, it is shown that the surface of the Li counter electrode was quite smooth after a certain amount of Li was plated/stripped on/from the electrode. This is thought to be because of the high-level cathodic stability of the RTIL PP13[TFSA]. The Li surface would react little with the PP13[TFSA] and a surface film whose properties are thought to be different from those produced in organic electrolytes is formed. However, the nickel (Ni) working electrode surface was coated with a coarsely textured black deposit after the cycling test, and the deposit may have been dead Li, which is often obtained by the dissolution of dendritic Li. For practical

* Corresponding author at: Research Institute for Ubiquitous Energy Devices, National Institute of Advanced Industrial Science and Technology (AIST), Midorigaoka 1-8-31, Ikeda, Osaka 563-8577, Japan. Tel.: +81 72 751 7932; fax: +81 72 751 9609.
E-mail address: hikari.sakaebe@aist.go.jp (H. Sakaebe).

0378-7753/$ – see front matter © 2010 Elsevier B.V. All rights reserved.
doi:10.1016/j.jpowsour.2010.12.023

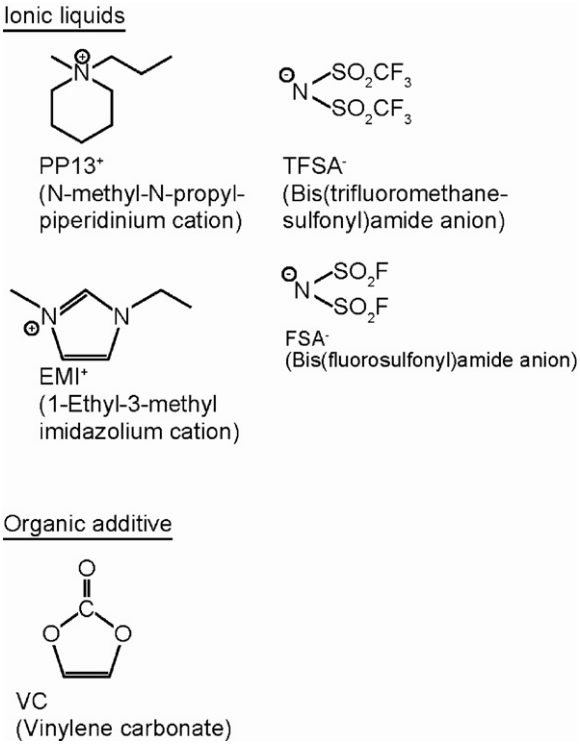

Fig. 1. Schematic illustration of the structure of RTIL cations and anions and the organic additive used in this study.

usage, dendritic formation on substrates other than Li electrodes should be suppressed.

Organic reagent addition to RTILs will alter the property of the surface film and may be followed by the planar growth of Li during charging, and, hence, cycling property improvement. Xu et al. reported that ethylene carbonate addition to PP13[TFSA] leads to a marked improvement in the cycling efficiency and cycle life [13].

As mentioned above, research on Li metal with RTIL electrolytes is now attracting considerable attention, but there are no reports on *in situ* morphological observation during Li electroplating in RTILs. *Ex situ* observation usually necessitates sample washing and subsequent transportation, resulting in a critical change of the sample surface state. In contrast, *in situ* observation does not require further washing or transportation. In the present study, we investigated the surface morphology of Li deposited in RTIL electrolytes with and without organic additives using *in situ* optical microscopy. As a result, fine non-dendritic particles were obtained using PP13[TFSA] with vinylene carbonate (VC).

2. Experimental

Electrolyte preparation was carried out in accordance with the previous reports [10,15]. PP13[TFSA] (Kanto Chemical) and EMI[FSA] (1-ethyl-3-methylimidazolium bis(fluorosulfonyl)amide, Kanto Chemical) were used as base RTIL electrolytes, and VC as an organic additive. Fig. 1 schematically

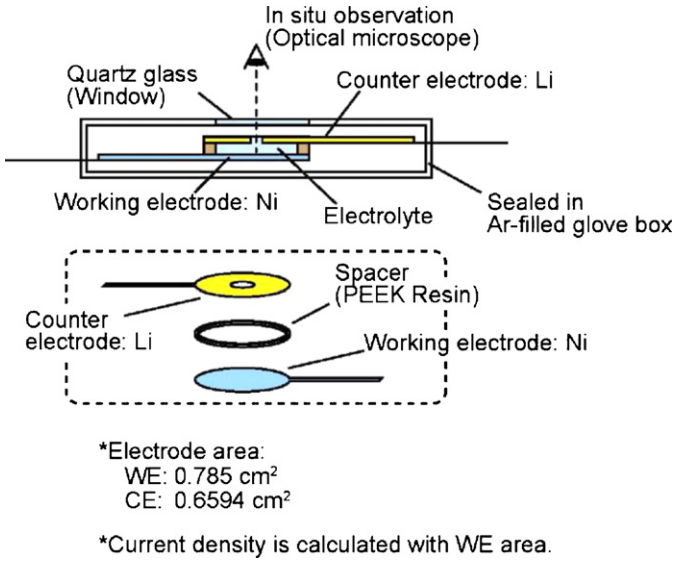

Fig. 2. Schematic illustration of a custom-made two-electrode cell used in this study.

shows the structure of the RTIL cations, anions, and the additive used in this study. Both RTILs were vacuum-dried overnight before use, and 0.32 mol kg^{-1} (≈10 wt.%, ≈0.46 mol dm^{-3}) and 0.69 mol kg^{-1} (≈25 wt.%, ≈1.0 mol dm^{-3}) of the supporting electrolyte LiTFSA (Kishida Chemical, 99.8%), which was vacuum-dried separately in advance, was added to the dried PP13[TFSA] and EMI[FSA], respectively. Then, the base electrolytes were prepared. For the electrolytes containing VC, 0.35 mol kg^{-1} (≈3 wt.%) of VC was added to each base electrolyte. This procedure was conducted in a dry room, and then the electrolyte was transferred into an argon (Ar)-filled glove box with a dew point below −75 °C (less than a 1-ppm water content), and with less than a 5-ppm oxygen content. The base electrolyte with PP13[TFSA] and EMI[FSA], and these electrolytes containing VC, are hereafter referred to as PP13TFSA, EMIFSA, PP13TFSA + VC, and EMIFSA + VC, respectively.

A schematic illustration of the custom-made two-electrode cell with a quartz glass window used for the experiment is shown in Fig. 2. Working and counter electrodes were Ni foil (Nilaco, 99.7%, 30-μm thickness) and Li thin film spattered on copper foil (Honjo metal, 50-μm Li thickness, 100-μm copper thickness), respectively. The spacer ring made of polyetheretherketone (PEEK) resin (10-mm inside diameter, 1.0-mm thickness) was inserted between the two electrodes, and both electrodes were pressed to the spacer ring to fix the distance between the two electrodes at 1.0 mm. A circular hole of 4 mm in diameter was punched in the center of the counter Li electrode for the *in situ* observation of the working electrode. The electrolytes were injected from this hole. The cell fabrication process was carried out in an Ar-filled glove box.

For the electrochemical control, a potentiostat (Iviumstat, Ivium) was used. The current density was 150 or 50 μA cm^{-2} and the charge amount was 3 C cm^{-2}, which is summarized in Table 1. During the electrodeposition of Li on the Ni working electrode,

Table 1
Condition of Li electrodeposition.

Condition	Electrolyte	Current density/μA cm^{-2}	Coulombs/C cm^{-2}	Deposition time/s
A	EMIFSA (VC-free)	150	3	20,000
B	EMIFSA + VC	150	3	20,000
C	PP13TFSA (VC-free)	50	3	60,000
D	PP13TFSA + VC	50	3	60,000
E	EMIFSA (VC-free)	50	3	60,000

the Ni working electrode surface was observed using an optical microscope.

The voltages of the cells were measured as the potentials of the working electrodes during Li electrodeposition. The working electrode surface was observed *in situ* with an optical microscope and images were taken every 60 s. After the electrodeposition of 3 C cm^{-2}, the sample cell was opened in the Ar-filled glove box and the working electrode was picked up and washed by flowing dimethyl carbonate (DMC, Tomiyama Pure Chemical). The washed working electrodes were transferred to a scanning electron microscopy (SEM) chamber using a custom-made transfer vessel, and the working electrode surface were observed by SEM.

At the last part of Section 4, we showed a supplementary X-ray photo-electron spectroscopy (XPS) spectra. The samples for XPS measurement was fabricated aside from the sample above. Coin-type three-electrode cells sealed in aluminum laminate films were fabricated following the literature [16]. Working, counter, and reference electrodes were Ni foil (Nilaco, 99.7%, 14 mm in diameter, 30 μm thickness), Li foil (Honjo metal, battery grade, 14 mm in diameter, 300 μm in thickness) pressed onto Ni foil, and a small Li chip attached on the end of a Ni tab, respectively. A two-ply separator consisting of glass fiber filter (Whatmann, GF/A) and polyolefin film (containing SiO_2 fine particles, 30 μm thickness, Nippon Sheet Glass) was wetted with either of the prepared electrolytes. The cell fabrication process was carried out in the Ar-filled glove box. After the electrodeposition of 3 C cm^{-2} with 50 μA cm^{-2} in current density, the sample cell was opened in the Ar-filled glove box and the working electrode was picked up and washed by flowing DMC. Then, XPS measurement was carried out using JPS-9010MX (JEOL), the background pressure of which was lower than 5×10^{-7} Pa. The X-ray source was Mg Kα operated at 10 kV and 10 mA. C 1s and O 1s regions were shown in this work, and were scanned under the following conditions: pass energy was 10 eV; step width was 0.1 eV; sampling time was 100 ms; and scan cycles were 10 times.

3. Results

3.1. Potential change during Li deposition

Fig. 3 shows the potential change during Li deposition in each electrolyte for a given current density, where these potentials were measured every 60 s. Before Li deposition, the potential of the Ni electrode was around 2.5 V. When Li deposition started, the potential dropped rapidly, but, in 120 s, the rapid drop stopped at around 1.0 V and the potential decreased slowly to 0 V. This slow decrease is thought to be caused by the decomposition of one or more electrolyte components or Li under potential deposition (UPD) [17,18]. The potentials of all samples reached 0 V in 500 s (Fig. 3a–d), but the sample with EMIFSA with a 50-μA cm^{-2} current density needs a longer time, 1740 s, for the potential to reach 0 V (Fig. 3e). In each graph, a small circle was plotted at the point where the potential reached 0 V, and the deposition time was noted nearby. After reaching 0 V, the potential was kept at 0 V until the deposition treatment was finished at 20,000 or 60,000 s, indicating that the redox reaction of Li is a main reaction determining the potential and the working electrode was covered with Li. In detail the plateau potential is slightly less than 0 V, that is, −0.02 to −0.10 V. This subtle negative shift from 0 V is caused by the over-potential on both electrodes and the IR drop.

When the EMIFSA (VC-free) sample is compared with the EMIFSA + VC sample, the potential reached 0 V earlier for EMIFSA + VC, indicating that EMI[FSA] decomposition might be suppressed by VC addition by forming a certain film consisting of decomposed VC on the metal surface (Fig. 3a and b). When the

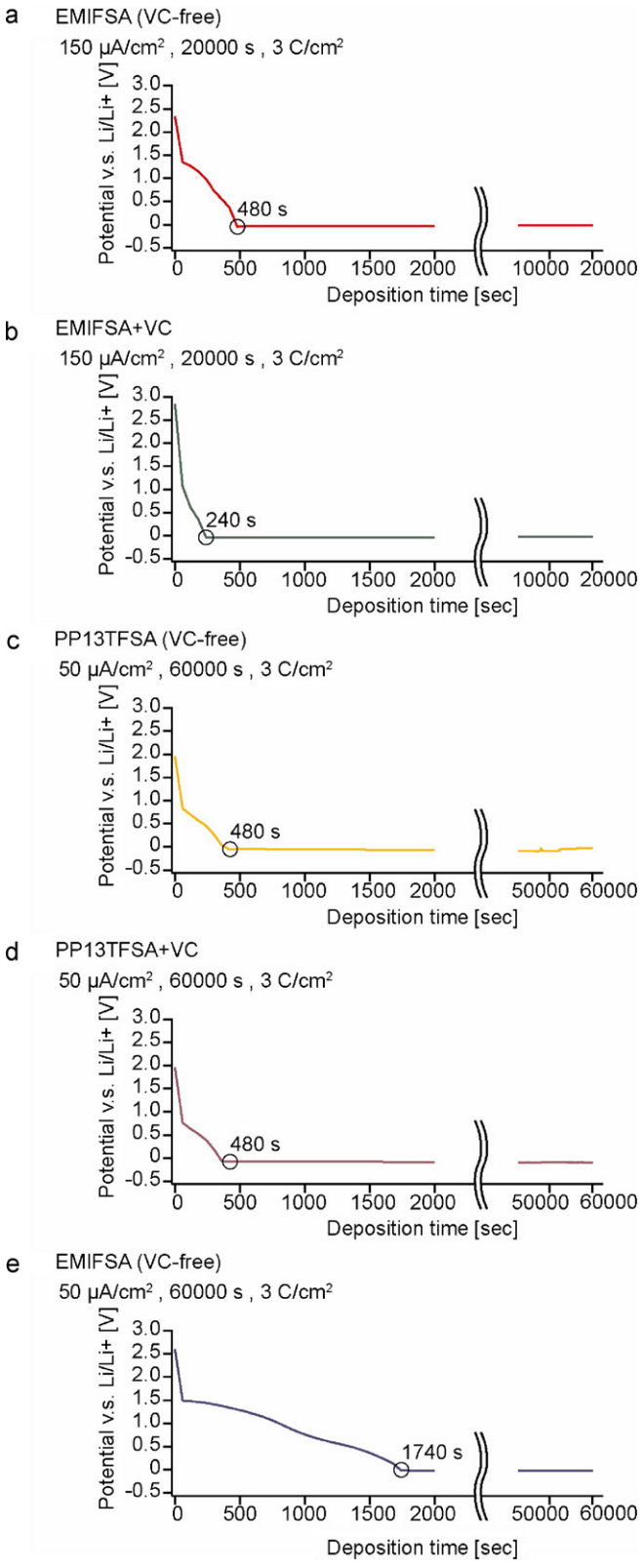

Fig. 3. Potential time dependency during Li electrodeposition under the conditions summarized in Table 1. The electrolytes were (a and e) EMIFSA (VC-free), (b) EMIFSA + VC, (c) PP13TFSA (VC-free), and (d) PP13TFSA + VC. The current densities were (a and b) 150 μA cm^{-2} and (c, d, and e) 50 μA cm^{-2}.

PP13TFSA (VC-free) sample is compared with the PP13TFSA + VC sample, there is little difference between the two (Fig. 3c and d).

3.2. In situ observation by optical microscopy

Optical microscopic images were taken for the *in situ* observation of the working electrode surface until 3 C cm^{-2} of electrodeposition had been completed. For each case, there was no change on each working electrode surface before the potential reached 0 V, and, just after the potential reached 0 V, some deposits were observed on the surface (not shown). They are considered to be Li deposits. Then, the number of deposits increased, and the size of some deposits enlarged. Particularly for EMIFSA and EMIFSA + VC samples, once a deposit grew larger than the other neighboring deposits to a certain extent, the larger deposit continued to grow more and the neighbors grew little from then on. Fig. 4 displays the optical microscopic images taken after 3 C cm^{-2} of electrodeposition for all samples. This tendency is apparent in the case of EMIFSA and EMIFSA + VC from the image (Fig. 4a, b, and d). There is large distribution in particle size; for example, for the case of EMIFSA, some large particles are 200 μm in diameter, and some small particles are less than 20 μm in diameter. Here we should note that the current density has negligible effect on the dendrite formation at the given current range, which is supported by the comparison of Fig. 4a and e. In contrast, for PP13TFSA and PP13TFSA + VC, the distribution in particle size is very small, with sizes around 5 nm (Fig. 4c and d), which can be also confirmed by SEM images, which are described later.

3.3. Observation by SEM

Fig. 5 displays the SEM images for each sample after Li deposition. Some particles are removed by DMC washing. There is smaller amount of particles especially on the SEM images of EMIFSA and EMIFSA + VC samples, than on the optical images. This is one disadvantage of *ex situ* observation, but the detailed shape of residual particles is precisely observed by SEM. The particles on the PP13TFSA and PP13TFSA + VC samples are very fine, and the particles on other samples are much coarser. When the difference between the two RTILs, EMI[FSA] and PP13[TFSA], is focused on, the particle sizes are much smaller for the sample with electrolytes using PP13[TFSA] than using EMI[FSA]. It is apparent from a comparison between the results for the conditions (A (EMIFSA, 150 μA cm^{-2})), (C (PP13TFSA, 50 μA cm^{-2})), and (E (EMIFSA, 50 μA cm^{-2})) (See Table 1 to confirm the conditions.), that the smaller particle size is not caused by a larger current density. Both average particle sizes for conditions (A) and (E) are much larger than for condition (C).

The particle shape is dendritic for the samples EMIFSA, EMIFSA + VC, and PP13TFSA, but granular for the sample of PP13TFSA + VC. Here we can also state that that the current density has negligible effect on the dendrite formation at the given current range, which is supported by the comparison of Fig. 5a and e. Dendritic growth was suppressed and planar growth was promoted using PP13[TFSA] and VC as additives.

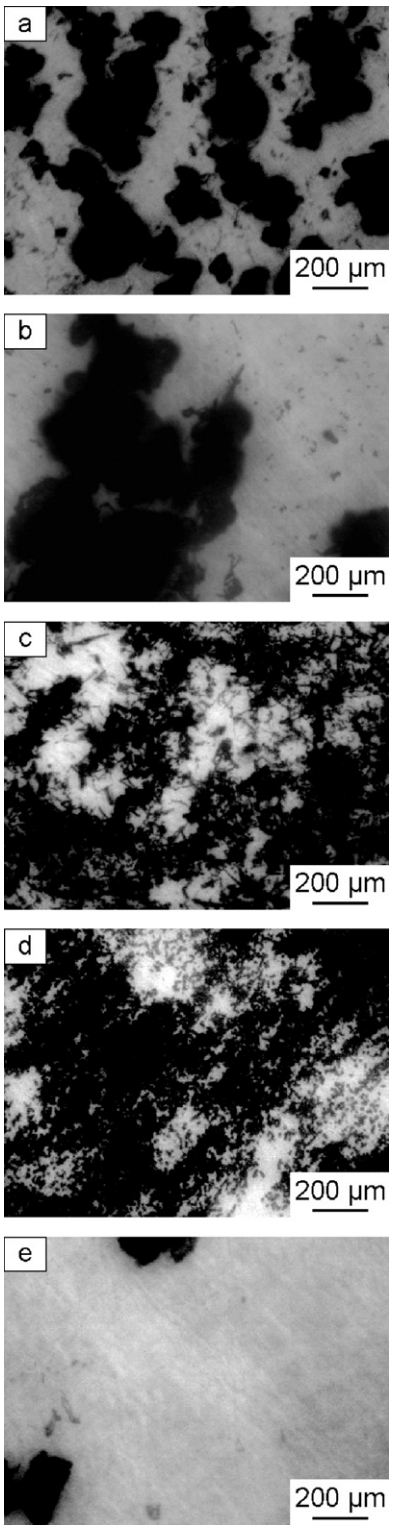

Fig. 4. Optical microscopic images after Li electrodeposition under the conditions summarized in Table 1. The electrolytes were (a and e) EMIFSA (VC-free), (b) EMIFSA + VC, (c) PP13TFSA (VC-free), and (d) PP13TFSA + VC. The current densities were (a and b) 150 μA cm^{-2} and (c, d, and e) 50 μA cm^{-2}.

4. Discussion

Table 2 summarizes the size and shape of particles obtained on each sample based on optical microscopy and SEM observation. As is mentioned in Section 1, the shape of the deposited Li is affected by the surface film formed by the reaction of Li with electrolytes. Aurbach's group suggested a mechanism of dendritic growth of Li deposits during charging [1]. First, the volume of lithium changes by deposition and a crack forms when the volume change is not uniform on the surface. This nonuniform volume change on the surface is caused by the inhomogeneous Li deposition. Second, the Li deposits more through the crack because Li ion diffusion is easier near the crack than through the surface film, resulting in the dendritic morphology. Here, it is important to clarify what causes the inhomogeneous Li deposition on the surface. This is mainly because the surface film is nonuniform from the view point of the thickness

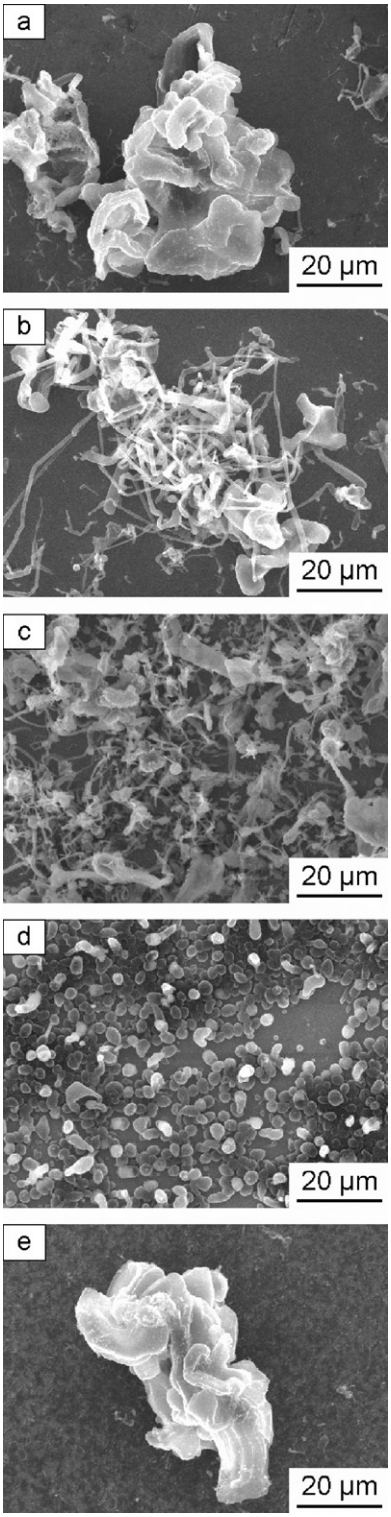

Fig. 5. SEM images after Li electrodeposition under the conditions summarized in Table 1. The electrolytes were (a and e) EMIFSA (VC-free), (b) EMIFSA + VC, (c) PP13TFSA (VC-free), and (d) PP13TFSA + VC. The current densities were (a and b) 150 μA cm^{-2} and (c, d, and e) 50 μA cm^{-2}.

or the density. Thus, to prevent inhomogeneous Li deposition, formation of uniform surface film is needed. Kanamura et al. presented one solution to this problem: their group used a trace of aqueous HF as an additive [3]. In electrolytes with HF, when the volume change is caused by Li deposition and the surface film cracks, the fresh Li rapidly reacts with HF and, hence, forms a new compact surface film. As a result, the deposited Li has a planar morphology, not a dendritic one.

Table 2
Particle size and shape of each sample.

	Without additive	With additive (VC)
EMI[FSA] (150 μA cm^{-2})	Coarse dendrite (POOR)	Coarse dendrite (POOR)
PP13[TFSA] (50 μA cm^{-2})	Fine dendrite	Fine granular particle (GOOD)
EMI[FSA] (50 μA cm^{-2})	Coarse dendrite (POOR)	–

Table 3
Viscosity of the electrolytes used in this study. The data was measured at 25 °C.

Electrolyte	Viscosity/cP
EMIFSA (VC-free)	39.3
EMIFSA + VC	35.6
PP13TFSA (VC-free)	320.9
PP13TFSA + VC	182.4

PP13[TFSA] has a high-level cathodic stability, although EMI[FSA] shows low-level cathodic stability; the cathodic limit of PP13[TFSA] and EMI[FSA] is −3.4 and −2.5 V vs. Fc/Fc$^+$, respectively [14]. Considering that the potential of Li/Li$^+$ is around −3.3 V *vs.* Fc/Fc$^+$, PP13[TFSA] is considered to decompose little at the Li plating potential. Here, we should note that the electrochemical window of an RTIL may change when an electrolyte such as Li[TFSA] was added to the RTIL. If you compare the potential change for EMIFSA and PP13TFSA under the same current condition (Fig. 3c and e), the electrolyte decomposes more for EMIFSA, which is confirmed by the longer time for the potential to reach 0 V. Larger particles are obtained for EMIFSA than for the case of PP13TFSA.

Table 3 summarizes the viscosity of the four electrolyte measured using a cone-plate type viscometer (Brookfield DV-III+). Taking that PP13TFSA + VC suppressed dendrite formation into account, the lower viscosity seems to contribute to the suppression. But, EMIFSA and EMIFSA + VC, which have lower viscosity than PP13TFSA + VC do not suppress the dendritic formation. Then, some factors but viscosity affect the particle shape.

Comparing EMIFSA with EMIFSA + VC (Fig. 3a and b), VC addition may cause the suppression of electrolyte decomposition, which is also reported for the case with VC addition to the organic electrolyte [6]. However, the effect of VC addition to EMI[FSA] on the morphology of the deposited Li is very small, that is, it also yielded coarse dendritic Li. For the cases of EMIFSA and EMIFSA + VC, EMI[FSA] decomposes and forms a films. The films formed for these cases are so similar to each other that they result in the similar particle formation. This is ensured by the comparison of the spectrum obtained from the EMIFSA XPS sample and EMIFSA + VC XPS sample (Fig. 6a and b). There is little difference between the spectra of the EMIFSA XPS sample and EMIFSA + VC XPS sample. Then, the formed films on these samples are considered as schematically illustrated in Fig. 7a and b. The films have the decomposed EMIFSA as a main component, and the film for the EMIFSA + VC sample has a partial area derived from VC or its decomposed material. These are similar to each other so that they forms similar particles.

Comparing PP13TFSA with PP13TFSA + VC (Fig. 3c and d), the effect of VC addition on the potential change tendency is very small. This may be because PP13[TFSA] is very stable at cathodic condition such as 0 V *vs.* Li/Li$^+$ in potential. However, the effect of VC addition to PP13TFSA is markedly large. The morphology of the deposits is fine and granular when VC is added to PP13TFSA. Considering the effect of VC addition to PP13TFSA, the main component of the film is decomposed VC, and the film should be uniform.

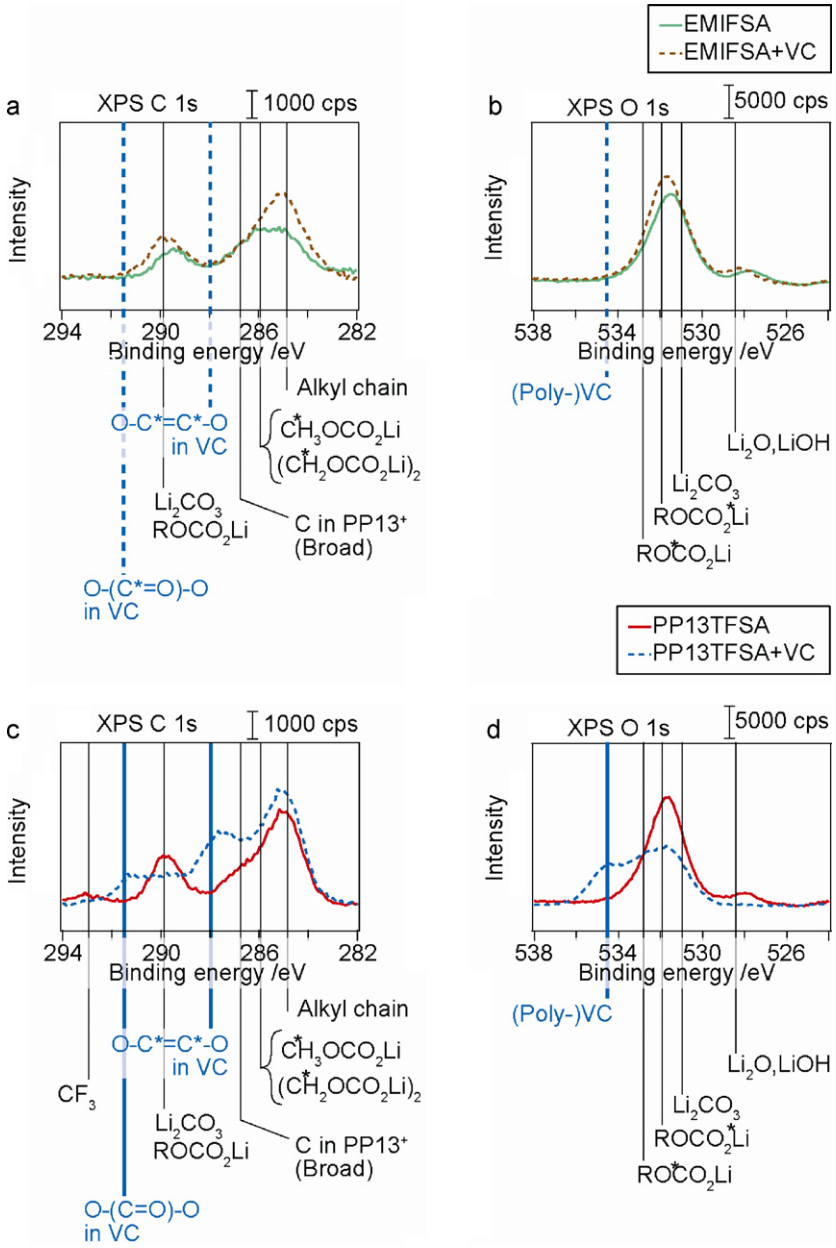

Fig. 6. XPS spectrum in the region of C 1s (a and c) and O 1s (b and d) for the electrolytes of (a and b) EMIFSA and EMIFSA + VC, and (c and d) PP13TFSA and PP13TFSA + VC.

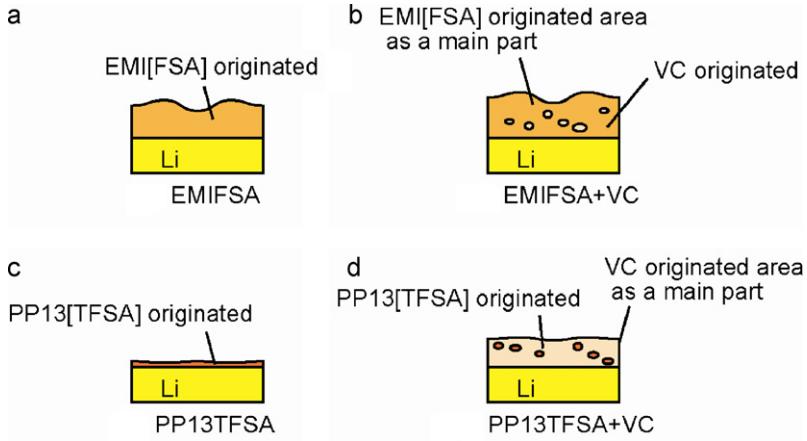

Fig. 7. Schematic illustration of the films formed on the sample surface for (a) EMIFSA, (b) EMIFSA + VC, (c) PP13TFSA, and (d) PP13TFSA + VC.

Moreover, the film may be soon restored even when a crack is formed, which is considered to be due to the short period needed for the potential to reach 0 V for the case of PP13TFSA + VC (Fig. 6c and d). When the spectrum obtained from the EMIFSA XPS sample and EMIFSA + VC XPS sample is compared (Fig. 6a), EMIFSA + VC XPS sample has peak contributions around 2391.5 and 288 eV in C 1s region, and 534.5 eV in O 1s region. These peak contributions can be attributed to be O–(C*=O)–O, O–C*=C*=O in VC, and (poly-)VC. Considering that PP13[TFSA] is very stable under the condition of this study, the film for the PP13TFSA sample is very thin, and the film for the PP13TFSA + VC contains VC-derived part as a main component, which is schematically illustrated in Fig. 7c and d. For the case of PP13TFSA + VC, the film covered the surface with uniformity and result in the uniform and granular Li deposition.

5. Conclusion

Dendritic particles were obtained for the case of EMI[FSA] with and without VC, and PP13[TFSA] without VC, while fine non-dendritic particles were obtained for the case of PP13[TFSA] with VC. The reason for the suppression of Li dendritic growth was discussed; a uniform film mainly consisting of decomposed VC was formed on the surface for the case of PP13[TFSA].

Acknowledgment

This work was supported by JST, CREST.

References

[1] D. Aurbach, E. Zinigrad, Y. Cohen, H. Teller, Solid State Ionics 148 (2002) 405.
[2] K. Kanamura, S. Shiraishi, H. Tamura, Z. Takehara, J. Electrochem. Soc. 141 (1994) 2379.
[3] K. Kanamura, S. Shiraishi, Z. Takehara, J. Electrochem. Soc. 143 (1996) 2187.
[4] S. Shiraishi, K. Kanamura, Z. Takehara, Langmuir 13 (1997) 3542.
[5] M. Ishikawa, S. Machino, M. Morita, J. Electroanal. Chem. 473 (1999) 279.
[6] D. Aurbach, K. Gamolsky, B. Markovsky, Y. Gofer, M. Schmidt, U. Heider, Electrochim. Acta 47 (2002) 1423.
[7] H. Ota, K. Shima, M. Ue, J. Yamaki, Electrochim. Acta 49 (2004) 565.
[8] H. Ota, Y. Sakata, Y. Otake, K. Shima, M. Ue, J. Yamaki, J. Electrochem. Soc. 151 (2004) A1778.
[9] S. Zhang, J. Power Sources 162 (2006) 1379.
[10] H. Sakaebe, H. Matsumoto, Electrochem. Commun. 5 (2003) 594.
[11] P. Howlett, D. MacFarlane, A. Hollenkamp, Electrochem. Solid State Lett. 7 (2004) A97.
[12] H. Sakaebe, H. Matsumoto, K. Tatsumi, J. Power Sources 146 (2005) 693.
[13] J. Xu, J. Yang, Y. NuLi, J. Wang, Z. Zhang, J. Power Sources 160 (2006) 621.
[14] H. Matsumoto, H. Sakaebe, K. Tatsumi, M. Kikuta, E. Ishiko, M. Kono, J. Power Sources 160 (2006) 1308.
[15] H. Sakaebe, H. Matsumoto, K. Tatsumi, Electrochim. Acta 53 (2007) 1048.
[16] H. Sano, H. Sakaebe, H. Matsumoto, J. Electrochem. Soc., in press, doi:10.1149/1.3532054.
[17] L.-F. Li, D. Totir, Y. Gofer, G.S. Chottiner, D.A. Scherson, Electrochim. Acta 44 (1998) 949.
[18] M. Moshkovich, Y. Gofer, D. Aurbach, J. Electrochem. Soc. 148 (2001) E155.